# Supersite of immune vulnerability on the glycosylated face of HIV-1 envelope glycoprotein gp120

Published in final edited form as:
*Nat Struct Mol Biol*. 2013 July ; 20(7): . doi:10.1038/nsmb.2594.

# Supersite of immune vulnerability on the glycosylated face of HIV-1 envelope glycoprotein gp120

**Leopold Kong**[1,2], **Jeong Hyun Lee**[1], **Katie J. Doores**[2,3,4], **Charles D. Murin**[1], **Jean-Philippe Julien**[1,2], **Ryan McBride**[5], **Yan Liu**[6], **Andre Marozsan**[7], **Albert Cupo**[7], **Per-Johan Klasse**[7], **Simon Hoffenberg**[8], **Michael Caulfield**[8], **C. Richter King**[8], **Yuanzi Hua**[1,2], **Khoa M. Le**[2,3], **Reza Khayat**[1], **Marc C. Deller**[1,9], **Thomas Clayton**[1,9], **Henry Tien**[1,9], **Ten Feizi**[6], **Rogier W. Sanders**[7,11], **James C. Paulson**[5], **John P. Moore**[7], **Robyn L. Stanfield**[1,2], **Dennis R. Burton**[2,3,4,12], **Andrew B. Ward**[1,2,12], and **Ian A. Wilson**[1,2,12,13]

[1]Department of Integrative Structural and Computational Biology, The Scripps Research Institute, La Jolla, California, USA [2]International AIDS Vaccine Initiative Neutralizing Antibody Center, The Scripps Research Institute, La Jolla, California, USA [3]Department of Immunology and Microbial Science, The Scripps Research Institute, La Jolla, California, USA [4]Ragon Institute of Massachusetts General Hospital, Massachusetts Institute of Technology, and Harvard, Cambridge, Massachusetts, USA [5]Department of Cell and Molecular Biology, The Scripps Research Institute, La Jolla, California, USA [6]Glycosciences Laboratory, Department of Medicine, Imperial College London, London, UK [7]Weill Medical College of Cornell University, New York, New York, USA [8]International AIDS Vaccine Initiative Design and Development Laboratory, Brooklyn, New York, USA [9]Joint Center for Structural Genomics, http://www.jcsg.org, USA [11]Department of Medical Microbiology, Academic Medical Center, Amsterdam, Netherlands [12]Scripps Center for HIV/AIDS Vaccine Immunology & Immunogen Discovery, The Scripps Research Institute, La Jolla, California, USA [13]Skaggs Institute for Chemical Biology, The Scripps Research Institute, La Jolla, California, USA

## Abstract

A substantial fraction of broadly neutralizing antibodies (bnAbs) in certain HIV-infected donors recognizes glycan-dependent epitopes on HIV-1 gp120. Here, we elucidate how bnAb PGT 135 recognizes its Asn332 glycan-dependent epitope from its crystal structure with gp120, CD4 and Fab 17b at 3.1 Å resolution. PGT 135 interacts with glycans at Asn332, Asn392 and Asn386, using long CDR loops H1 and H3 to penetrate the glycan shield to access the gp120 protein surface. Electron microscopy reveals PGT 135 can accommodate the conformational and chemical diversity of gp120 glycans by altering its angle of engagement. The combined structural studies of PGT 135, PGT 128 and 2G12 show this Asn332-dependent epitope is highly accessible and much more extensive than initially appreciated, allowing for multiple binding modes and varied angles of approach, thereby representing a supersite of vulnerability for antibody neutralization.

Correspondence should be addressed to D. R. B (burton@scripps.edu), A.B.W. (abward@scripps.edu) or I.A.W. (wilson@scripps.edu).

**Accession Codes** Coordinates and structure factors for Fab PGT 135 and its complex with gp120, CD4 and 17b have been deposited with the Protein Data Bank under accession codes 4JM4 and 4JM2, respectively. The Fab PGT 135/SOSIP.664 trimer EM reconstruction density has been deposited with the Electron Microscopy Data Bank under accession code EMD-2331.

**Author Contributions** Project design by L.K., K.J.D. J.-P.J., R.L.S, D.R.B., A.B.W., I.A.W.; X-ray experimental work by L.K., J.-P.J., Y.H., R.S.L.; EM experimental work by J.H.L., C.D.M., R.K., A.B.W.; glycan array experimental work by R.M., J.C.P., Y.L., T.F.; mutational experimental work by K.J.D., K.M.L.; Env trimer reagents from A.M., A.C., P.-J.K., S.H., M.C., C.R.K., R.W.S. and J.P.M.; robotic crystallization screening at the JCSG by M.C.D., T.C. and H.T.; manuscript written by L.K., J.H.L., K.J.D., R.L.S., J.P.M., D.R.B., A.B.W., and I.A.W. All authors were asked to comment on the manuscript.

The human immune system initially generates strain-specific neutralizing antibodies to HIV-1 that recognize only a fraction of the massively diverse mutational variants of its envelope glycoprotein (Env)[1]. In the infected host, the virus diversifies extensively and escapes from these narrowly focused antibodies. Strong selection pressure drives variation in its exposed surfaces, including its five hypervariable loops (V1-V5) and around 27 *N*-linked glycans that cover most of the gp120 envelope glycoprotein surface[2-4]. Despite this extraordinary sequence variation and "evolving glycan shield", broadly neutralizing activity is found in 5-25% of donor sera after 2-3 years of infection[5,6]. However, by this time, the virus has firmly established itself, overwhelming even broadly neutralizing responses. Nevertheless, elicitation of such responses by a vaccine prior to virus exposure may lead to prophylactic protection against HIV-1.

Given that neutralizing antibody selection pressure shifts glycosylation sites on the virus during the course of infection[2], it is reasonable to assume that these antibodies may not only be targeting protein surfaces near glycans, but also the glycans themselves. This notion is supported by observations of serum neutralizing activity that is dependent on the presence of the glycan attached to Asn332[7-10] and by the recent discovery of several broadly neutralizing antibodies (bnAb) that interact with gp120 in a glycan-dependent manner. Four antibodies isolated from different HIV-1 infected donors and derived from different germline families, PGT 121[11], 2G12[12], PGT 128[13] and PG9[14], have been structurally characterized in complex with individual glycans, a gp120 outer domain fragment, and a scaffolded glycopeptide, respectively. A number of other glycan-dependent bnAbs, including PG16 and PGT 121-123, 130-131 and 142-145 (n.b. the PGT antibodies are grouped according to their predicted shared germline precursor), await structural characterization in complex with Env[15,16].

To further elucidate the bnAb target around Asn332, we conducted structural and functional analysis of PGT 135, an Asn332 (N332) glycan-dependent bnAb isolated from an individual whose serum has one of the highest neutralization breadths known[16,17]. The PGT 135 epitope includes three glycans and protein segments that differs substantially from other Asn332-dependent epitopes and enables PGT 135 accommodation of HIV-1 Env glycan heterogeneity through some variation its angle of approach to the gp120 surface. Hence, the Asn332-dependent epitope constitutes a major site of vulnerability on the glycosylated face of gp120 that can be accessed by antibodies from different germline precursors using completely different modes of recognition and, most likely, different mechanisms of neutralization.

## Results

### Structural characterization of PGT 135 binding to gp120

To elucidate the interaction with gp120, we tested PGT 135 Fab complexed with a number of gp120 constructs and additional ligands for crystallization. The additional ligands included soluble CD4 receptor and Fabs recognizing gp120 to increase the chances of crystallization[18]. Crystals of a quaternary complex (i.e. four protein components) consisting of PGT 135 Fab, JR-FL core gp120, CD4 D1D2 and 17b Fab (Fig. 1) diffracted to 3.1 Å resolution (Table 1), while unliganded Fab135 crystals diffracted to 1.75 Å (Table 1). The JR-FL gp120 monomeric core bound to PGT 135 Fab with high affinity [82 nM by ITC (Supplementary Table 1)], but the corresponding virus was only weakly neutralized by PGT 135 IgG unless specific mutations were introduced into the V1-V2 loops, which are >25 Å away from the epitope in the monomeric gp120 structure and probably affect binding indirectly by impacting trimer interactions (Fig. 2)[19]. Nevertheless, the weak neutralization that we observed correlates with an approximate μM binding affinity for the Env trimer. A number of bnAb-Env complexes in this affinity range have been structurally elucidated, e.g.

b12 with a stabilized gp120 core construct[20] and PG9 with V1-V2 loop scaffolds[14] and these structures are consistent with many published findings on Env biology.

The crystal structure shows that CD4, 17b and PGT 135 are bound to gp120 in nearly orthogonal orientations (Fig. 1a). After partially deglycosylating the gp120/PGT 135 complex by endoglycosidase H (EndoH) prior to crystallization, we observed only single *N*-acetylglucosamine (GlcNAc) moieties in the gp120 electron density at Asn339, Asn362, Asn448, Asn262 and Asn276, whereas high mannose (Man) glycans interacting with PGT 135 were protected and we observed density for $GlcNAc_2Man$ at Asn386 (N386), $GlcNAc_2Man_6$ at Asn332 and $GlcNAc_2Man_8$ at Asn392 (N392). When compared to its unliganded structure, PGT 135 does not undergo any large conformational changes [0.4 Å Cα root-mean-square deviation (RMSD) between Fab variable domains] (Supplementary Fig. 1a-b). The gp120 structure is also highly similar in both the PGT 135-CD4-17b-$gp120_{JRFL}$ and the CD4-17b-$gp120_{HXBC}$ complexes[20] (0.5 Å Cα RMSD), suggesting that PGT 135 does not induce any further conformational changes when it binds to gp120. This inference was corroborated by ITC data: the ΔG, ΔH and TΔS values for PGT 135 binding to unliganded gp120 and to the gp120-CD4 complex were nearly equivalent (Supplementary Table 1). Therefore, evidence that PGT 135 neutralizes virus by inducing conformational changes in gp120 or by direct inhibition of CD4 binding is lacking. However, the PGT135 neutralization mechanism still remains unclear although we note that the PGT 135 epitope also involves residues from the V4 loop. In another study, an anti-FLAG antibody, which neutralizes recombinant virus containing a FLAG insert in the V4 loop[21], appears to function via nonspecific steric coverage of the virion[22] instead of blocking functionally important surfaces such as the CD4 binding site.

PGT 135 engages gp120 primarily via a long 18-residue CDR H3 loop, which has 10 amino-acid insertions after position 100 (n.b. the average human CDR H3 is 13 residues using the Kabat definition of H95-H102[23]), and an extended CDR H1 loop containing a rare 5 amino-acid insertion not present in the predicted germline sequence (Supplementary Fig. 2); both CDR loops protrude approximately 20 Å from the $V_H$ surface, comparable to the length of high mannose *N*-linked glycans. The $V_H$ CDR loops in unliganded PGT 135 converge to form a highly hydrophobic horseshoe-shaped surface consisting of Trp34 from CDR H1, Trp53 from H2, and Val100-FMLVP-Ile100F from H3 (Supplementary Fig. 1d). A salt bridge between Arg54 on the tip of H2 and Glu33 near the top of the H1 loop insertion helps hold these loops in place. These features remain intact after binding to gp120 (Supplementary Fig. 1c).

PGT 135 buries a complex epitope consisting of 438 $Å^2$ of protein and 1010 $Å^2$ of glycan surface on gp120 (Fig. 1 and Supplementary Table 2), which is larger than the typical antibody footprint (~700-900 $Å^2$). 83 percent of the protein-protein buried surface involves side chains on gp120 (Supplementary Table 2) in contrast to PG9 and PGT 128 that rely primarily on backbone interactions with V1-V2 and V3, respectively, to form main-chain β-strand associations[13,14]. The CDR H1 and H3 tips primarily contact gp120 β-strand 19, which connects the V4 loop to β-strand 20, as part of the bridging sheet (Fig. 1b), and adjacent β-strand 13, between V3 and α-helix 2, where His330 is particularly important for binding and neutralization (Supplementary Table 2-3). On the gp120 V4 loop, Glu409 interacts with CDRs L2 and H3, forming a protein-protein interaction zone that is discontinuous from the rest of the contacts. The CDR H1 insertion allows access to the protein surface around the Asn386 glycan ($GlcNAc_2Man$), which separates the PGT 135 epitope from the CD4 binding site. Trp34 on the tip of the CDR H1 insertion interacts with the Asn386 glycan. Coincidentally, bnAb b12 also contacts residues near the Asn386 glycan via CDR H3 Trp100, which occupies a similar position to PGT 135 H1 Trp34[20]. Deletion of the H1 insertion significantly reduced PGT 135 binding and neutralization of different

HIV-1 isolates (Fig. 2b-c), suggesting that this extended loop is important for the antibody-antigen interaction.

The large glycan binding surface of PGT 135 is created by the CDR loops draping themselves across the entire length of the *N*-linked glycans at Asn392 (547 $Å^2$) and Asn332 (365 $Å^2$), where multiple van der Waals interactions and hydrogen bonds are made from the mannose sugars at the tips to the GlcNAc moieties at the stem (Fig. 1, Fig. 3 and Supplementary Table 2, 4-7). The Asn386 glycan interaction is significantly less (99 $Å^2$, two van der Waals interactions with H1) than with the Asn392 and Asn332 glycans, but nonetheless critical for neutralization of various HIV-1 strains (Fig. 3d), (Supplementary Tables 3-7). Interestingly, the Asn392 and Asn332 glycans interact with opposite faces of PGT 135 CDR H3 in a bifurcated manner reminiscent of bnAb PG9 and PGT 128 binding to dual glycans on epitope-scaffolded V1-V2 loops (PG9) or gp120 outer domain (PGT 128), respectively (Fig. 3a). However, unlike these other bnAbs, whose interacting glycans are on adjacent β-strands, the two glycans interacting with PGT 135 CDR H3 are on independent β-strands separated by β-strand 19 (Fig. 1). $V_L$ also contacts the Asn332 glycan via CDR L3 on one side of $V_L$, whereas CDR L2, and $V_L$ framework regions 2-3 on the opposite side interact with the Asn392 glycan (Fig. 1).

## Glycan specificity of PGT 135

*N*-linked glycans exhibit multiple levels of heterogeneity, arising from variable positioning of the glycosylation sequons on gp120, differential processing by Golgi enzymes, and conformational flexibility[24,25]. To understand how PGT 135 achieves relatively broad neutralizing activity despite dependence on heterogeneous glycans, we employed virus neutralization and binding assays based on virus and gp120s from different strains with various *N*-linked glycosylation knockouts, along with glycan arrays and different expression systems (Fig. 3b-d). These results were compared with analysis of the glycans in the crystal structure of a partially deglycosylated PGT 135 complex. Crystallization required partial deglycosylation of the complex, which we carried out with the rationale that EndoH will preferentially cleave the more exposed and flexible N-linked glycans[26] that are not protected by PGT 135 binding (Supplementary Fig. 3d).

Pseudoviruses prepared from mammalian 293T cells (complex, hybrid and oligomannose glycans) or 293S cells ($Man_{5\text{-}9}GlcNAc_2$ oligomannose glycans) had similar PGT 135 neutralization profiles (Fig. 3c). These results are consistent with the crystal structure, which shows interaction only with an oligomannose glycan patch on gp120[27] that would be present when gp120 is expressed in either cell line, and validate the use of 293S cells to produce the gp120 for the crystal study. In contrast to 2G12 and PGT 128, PGT 135 also neutralized pseudoviruses from cells treated with N-butyldeoxynojirimycin (NB-DNJ), which results in either missing or glucosylated (i.e. masked) D1 arms of N-linked glycans[28]. This observation is also consistent with the crystal structure because PGT 135 does not interact with the Asn332 glycan D1 arm and only with the second mannose residue of the Asn392 glycan D1 arm, which would not be affected by NB-DNJ treatment (Fig. 3a). Also in contrast to 2G12 and PGT 128, adding kifunensine to the expression system, which limits glycan processing to $Man_9GlcNAc_2$, resulted in loss of neutralization by PGT 135. Again, the crystal structure is compatible with this outcome: modeling an additional mannose residue to the D2 arm of the $Man_8$ glycan at Asn392 would result in a severe steric clash (Supplementary Fig. 3a). The D2 arm of the $Man_6$ glycan at Asn332 is also sterically crowded, but may be able to accommodate a terminal mannose with some slight adjustment (Supplementary Fig. 3b). In contrast, the D3 arm of the Asn332 glycan is free from any steric clash with the antibody (Supplementary Fig. 3c).

Glycan array binding assays showed that PGT 135 recognized $Man_{7-9}$ glycans exclusively and bound to these with lower affinity than 2G12 and PGT128 (Fig. 3b). Although PGT 135 appears to bury extended glycan moieties in the binding site, most of the contacts are van der Waals interactions and the antibody makes only 4 hydrogen bonds to the Asn332 glycan. In contrast, PGT 128, which generated a substantially higher glycan binding signal on glycan arrays, makes 13 hydrogen bonds with the Asn332 glycan. The pattern of binding to these glycans is dependent on the density, clustering and conformation of the presented glycans; in a different glycan array format using non-covalently immobilized *N*-linked glycans as neoglycolipids that have an element of mobility, only $Man_8$ and $Man_7$ glycans without the terminal D2 mannose were recognized (Supplementary Table 8). The array analyses and kifunensine effect described above can be reconciled if binding to glycans other than Asn392, most likely Asn332, can occur via $Man_8$ or $Man_9$. While a homogenous display of glycans on an array is unlikely to mimic the actual presentation of the glycans on gp120, use of multiple arrays containing different coupling chemistries and printing densities allows more opportunity to assess the glycan specificity of PGT 135.

Virus neutralization and binding assays revealed differential effects of these N-linked glycosylation sites on PGT 135 activity against different isolates of HIV-1 (Fig. 3d). Not surprisingly, Asn332 and Asn392 were required for all isolates tested because most of the antibody contacts are to these glycans. However, the requirement for Asn295 (N295) and Asn386 glycans, as well as His330 residue, on gp120, was strain dependent. Although the Asn295 glycan does not contact PGT 135 in the context of the JR-FL core gp120, these data suggest it may be recruited by the antibody in the context of other HIV-1 strains so that the epitope would be modified and strain-dependent. Thus, although the PGT 135 interaction is highly specific for particular glycoforms on gp120, it may also be promiscuous by exploiting a neighboring Asn295 glycan for recognition of some HIV-1 strains. By targeting the oligomannose patch on gp120 where the required glycoforms are present, while tolerating a certain range of alternate glycan positions, PGT 135 may acquire broad neutralizing breadth despite the heterogeneity seen in the Env glycan populations. Overall, the data point towards two general requirements for PGT 135 binding, with the caveat that any given isolate may deviate from the most common pattern of recognition: 1) high mannose glycans within the context of the tightly clustered high mannose patch on gp120 and 2) a D2 arm on the glycan at Asn392 lacking at least the terminal mannose residue.

## Structural explanation for neutralization breadth of PGT 135

PGT 135 can neutralize 33% of HIV-1 isolates at an $IC_{50}$ <50 ug $ml^{-1}$ using a 162 cross-clade virus panel, which is comparable to bnAb b12 (34%), but less than PGT 128 (72%)[7], although PGT 135 and 128 both recognize epitopes critically dependent upon the same highly conserved Asn332 glycan[7]. The variability of important residues and glycan sites was examined using 3045 aligned gp120 sequences (Los Alamos HIV Database). The sequence conservation of the essential elements necessary for gp120 binding agrees well with neutralization breadth (Supplementary Table 2). For PGT 128, glycans at Asn332 (73% conserved) and Asn301 (N301) (92% conserved) are critical for neutralization; both glycan motifs are present together in 69% of the sequences, which is close to the observed 72% neutralization breadth[7]. For PGT 135, glycans at Asn332, Asn392, Asn295, Asn386, and His330 (73%, 79%, 59%, 87%, and 71% conserved, respectively) are all important for neutralization (Supplementary Table 2). His330, Asn332 and Asn392 are all required for neutralization of all isolates tested (Fig. 3d) and these three sites are found concurrently in 50% of the sequences. However, PGT 135 recognition also requires Asn295 and Asn386 glycans in a strain-dependent manner. His330, glycans at Asn332, Asn392, and either Asn295 or Asn386 are found in 31% or 42% of the sequences, while His330 along with all four glycan motifs (332, 392, 295, and 386) is present in 26% of the sequences. The

observed neutralization breadth of PGT 135 is 33% of test isolates[7], suggesting that the dispensability of either Asn295 or the Asn386 glycans in certain strains enhances neutralization breadth compared to a requirement for all four glycans.

### PGT 135 interaction with gp120 trimer

We used electron microscopy (EM) to characterize PGT 135 Fab binding to a glycosylated clade A BG505 SOSIP.664 gp140 trimer[29]. Three Fabs were bound per trimer, with the gp120 protomers in a more closed conformation (Fig. 4a) than the more open conformation seen with CD4 binding site ligands[30]. The PGT 135 angle of approach to the gp120 epitope avoids any clash with neighboring gp120 protomers or interference with the CD4 binding site (Fig. 4a). The 2D class averages showed that PGT 135 occupies a distinct epitope from PGT 128, which also recognizes the Asn332 glycan (Fig. 4b), but we observed significant variance in the orientation of Fab PGT 135 relative to the trimer (Fig. 4c, Supplementary Movie 1). Principal component analysis (PCA) of the variance clearly illustrated some flexibility in the Fab PGT 135 interaction with the trimer compared to PGT 128 (Fig. 4d, Supplementary Movie 2). This increased variance for PGT 135 may represent a distribution of different angles of approach due to some slight shift between the interacting glycans or with the glycoforms it contacts (Fig. 4d). The use of alternative angles of approach may therefore reflect an immunologic countermeasure to some natural variation in the *N*-linked glycans that decorate the Env surfaces of different HIV-1 isolates.

## Discussion

Recent advances in our understanding of immune responses against HIV-1 Env have revealed that extremely potent, broadly neutralizing responses can be made against the glycosylated face of gp120, particularly around the Asn332 glycan. PGT 135, 2G12 and PGT 128 bnAbs are all dependent on the Asn332 glycan but have distinct binding motifs and quite different angles of approach, and yet their neutralization activity is not compromised (Fig. 5a). This scenario contrasts with antibodies whose binding footprints overlap the CD4 binding site where small differences in angle and relative position result in clashes with neighboring gp120s[31] and very different extents of neutralization from VRC01 (bnAb, 93% breadth) to F105 (non-neutralizing)[5]. Thus, these Asn332-dependent antibodies define a novel and unexpectedly broad supersite for neutralization (Fig. 5b), which encompasses 6 conserved glycans and the underlying protein surface.

Overall in comparing HIV-1 bnAbs that interact with glycans, PGT 135 is similar to PGT 128 and PG9 in its use of heavy chain CDR loops to penetrate through the glycan canopy to contact the underlying protein surface with PG9 uniquely using a hammerhead-shaped CDR H3 loop for the interaction. As with PGT 128, but not PG9, PGT 135 also relies on a second extended CDR loop on the heavy chain (H1 in PGT 135 and H2 in PGT 128) to contact antigen. Despite different amino-acid lengths, these extended CDR loops are at similar distances from the antibody (15-20 Å), reflecting the length of an *N*-linked glycan from the underlying protein surface. In contrast, 2G12 only contacts the outermost mannose residues of the interacting glycans, a feature that presumably results from its unusual $V_H$ domain-swap to attain high affinity binding.

In terms of the relative glycan positioning within the binding sites, we also observe some similarities. For Fabs PGT 135, PGT 128 and 2G12, the distances between the two major interacting glycans on the gp120 surface (measured between the asparagine-bound carbons of the protein proximal GlcNAcs of the glycans) are remarkably similar at around 18-20 Å. The PG9 glycans are also spaced similarly at 15 Å. These similarities in distances likely reflect constraints imposed by the dimensions of the Fab interacting surfaces, the

requirement that a CDR loop penetrate between glycans, and the density of the glycans on the gp120 surface.

Although three different bnAbs recognize the same Asn332 glycan, they contact chemically distinct surrounding surfaces. 2G12 binds to the glycan tips and is, therefore, highly dependent on the presence of the terminal mannose residues in a particular linkage. In contrast, PGT 135 and PGT 128 recognize the complete length of the glycan at Asn332, but approach from and interact with different sides of the glycan. Strikingly, the glycan conformation and orientation is largely unchanged in the PGT 135 and PGT 128 structures (Fig. 6a), despite the known conformational flexibility of glycans. This conformational stability confers the carbohydrate with two chemically distinct “faces” at the level of the entire glycan; a much more flexible glycan would not have such well-defined faces because its overall orientation and conformation would be rapidly changing. The Asn332 glycan faces are defined by the sum of the contributions from the apolar and polar faces of individual sugar rings that then determine the net polarity of the complete face. The sugar hydroxyl groups extend from the polar side of a sugar ring, thereby potentially mediating more hydrophilic-type interactions compared to the apolar face (Fig. 6b). Thus, some ‘rules’ for interaction with individual sugars have been established whereby aromatic residues, such as Trp, typically stack on the apolar face of sugars and hydrophilic and charged residues interact with the polar face and hydrogen bond with the ring hydroxyl groups[32].

We observed that PGT 135 interacts predominantly with an apolar face consisting of three individual apolar sugar ring faces and one polar sugar ring face (Fig. 6c) with 61% of the buried surface in the interaction mediated by the individual apolar faces. PGT 128 interacts with a predominantly polar face consisting of 5 individual polar sugar faces and 2 individual apolar sugar ring faces, with 58% of the buried surface mediated by the polar faces (Fig. 6d). Conversely, PGT 135 residues interacting with the apolar face of glycan 332 are predominantly hydrophobic (~64% of the buried surface area contacts are mediated by apolar residues), while PGT 128 residues are about equally hydrophobic and hydrophilic (~54% of the buried surface in the interaction are mediated by apolar residues. It should be noted that the apolar interactions, particularly ring stacking, would naturally involve much greater surface area than hydrophilic interactions. Similarly, PGT 128 interactions with the polar face of glycan 332, involve many more hydrogen bonds compared to PGT 135 (13 versus 4). Thus, we conclude that the different faces of the Asn332 glycan are an important determinant for antibody recognition of this supersite.

The discovery of bnAbs in a SHIV-infected macaque that depend on the Asn332 glycan, in addition to those described above in infected humans[7-9], raises the prospect that suitable immunogens that display these combined glycan and protein epitopes in an appropriate configuration can be tested as vaccine candidates in animal models for re-elicitation of similar glycan-dependent antibodies. Furthermore, a recent study showed that broadly neutralizing responses were raised against the Asn332 glycan in two human individuals initially infected with a virus initially lacking the Asn332 glycan, but which contained an Asn334 glycan that is present only when Asn332 is absent[9]. The Asn332 glycan emerges later in the infection, but the virus can revert back to the Asn334 glycan, resulting in escape from the immune response. Although most viruses have the Asn332 glycan (73%) rather than the Asn334 glycan (20% conserved), a vaccine may need to be capable of inducing responses to either glycan site.

It is still not clear why the Asn332 glycan is so dominant among antibodies targeting this supersite, but one possibility is that it is not only highly conserved (73%) and predominantly oligomannose, but also conformationally restrained by adjacent sugars. Indeed, the glycan Asn332 conformation is nearly identical in the crystal structures of PGT 128[13] and PGT 135

(Fig. 6), suggesting that the immune system is presented with a comparatively well-ordered glycan shield, at least for glycan Asn332. Heterogeneity of surrounding glycans may be accommodated, as suggested by the distribution of angles of approach utilized by PGT 135, and in the case of PGT 121 potentially being able to bind both high mannose and complex glycans[11]. One implication for vaccine design is that immunization with an antigen containing a heterogeneous mix of glycoforms and glycosylation sites may promote "promiscuous" antibodies that have greater neutralization breadth. However, this benefit may be countered by a dampened immune response, in which case different vaccination schedules and adjuvants would need to be tested. Ultimately, to mimic this supersite using rational vaccine design, such as epitope scaffolding[33,34], to create vaccine immunogens, one should carefully consider how to reconstitute a faithful representation of the glycan canopy with glycoforms that are similar to those in the intact Env trimer.

## Online Methods

### Expression and purification of PGT 135 and 17b Fab

PGT 135 Fab was expressed using a baculovirus system with SF9 cells as described previously in ref. 13. PGT 135 was purified from the cell supernatant first by anti-human lambda affinity chromatography followed by cation exchange chromatography and size exclusion chromatography using Superdex 200™ (GE Healthcare) as previously described[13]. Fab 17b was obtained from digesting IgG 17b with papain using a previously described protocol from ref. 12.

### Expression and purification of JRFL gp120 core

A JRFL gp120 core containing a short (mini) V3 region (residues 305-320 deleted and replaced by a proline residue as described in ref. 13) was cloned into a phCMV3 vector with an IgK secretion signal. This plasmid was used to transfect HEK 293S GnT1-/- (293S) cells using 293Fectin (Invitrogen) under serum free conditions. The protein was purified first through a *Galanthus nivalis* lectin column, followed by SEC with Superdex 200™ (GE Healthcare).

### Expression and purification of BG505 SOSIP.664 trimer

The HIV-1 clade A BG505 Env sequence and the construction of SOSIP.664 trimers[35] using the Env sequence of BG505.W6M.ENV.C2 (GenBank Accession ABA61516/DQ208458) designed with a T332N mutation[36] is described in ref. 29. The BG505 SOSIP.664 trimer was expressed and purified as previously described in ref. 13. The BG505 SOSIP.664 trimer was purified using a 2G12-coupled affinity matrix followed by passage through a sizing column.

### Crystallization and data collection

Unliganded PGT 135 Fab crystallized over a period of 28 days at 20 °C in a crystallization reagent consisting of 20% (w/v) PEG 8000, 0.1 M CHES, pH 9.5. Crystals were harvested and cryoprotected by a brief immersion in 70% well buffer, 30% glycerol, followed by immediate flash-cooling in liquid nitrogen. Data were collected at APS beamline 23ID-B (wavelength: 1.033 Å) at 100 K. Data were processed and scaled with HKL-2000[37]. Quaternary complexes of PGT 135 crystallized in 20% PEG 2000, 0.1 M Tris pH 7.0 (JCSG CoreSuite I Well C07) using our automated CrystalMation robotic system (Rigaku). An optimization screen was made around this condition and large single crystals were obtained from 16% w/v PEG MME 2000, Tris pH 7.87 using the Oryx8 Crystallization robot. Data were collected at the ALS beamline 5.0.2 (wavelength: 1.000 Å) at 100 K, and were processed and scaled with HKL-2000[37]. All data processing statistics are summarized in Table 1.

### Structure determination and refinement

The unliganded PGT 135 structure was determined by the molecular replacement method using Phaser with an unrelated Fab structure (PDB ID: 3KYM) as an initial model. For the quaternary complex, multiple components were used for phasing: 17b Fab (PDB ID: 2NXY), soluble CD4 (PDB ID: 2NXY), gp120 core (PDB ID: 2NXY) and high-resolution unliganded PGT 135 Fab as determined here. Model building was carried out using Coot-0.6.2 and refinement was implemented with the Phenix program[38]. See Supplementary Note for refinement details and Table 1 for final refinement statistics.

### Isothermal titration calorimetry

Isothermal titration calorimetry (ITC) binding experiments were performed using a MicroCal iTC200 instrument (GE). See Supplementary Note for details.

### gp120 binding ELISAs

Recombinant gp120 (250 ng) was immobilised directly onto flat bottom microtitre plates (Costar type 3690, Corning Inc.) at 4°C overnight. Antibody binding was determined as described above. Fold change in binding for PGT 135 mutants is summarized in Supplementary Table 9.

### Generation of pseudovirus

Pseudovirus was generated in HEK 293T or GnT1$^{-/-}$ deficient 293S cells as described previously[39]. Glycosidase inhibitors were added at the time of transfection and were used alone or in combination at the following concentrations as described in ref. 13: 25 μM kifunensine and 2 mM *N*-butyldeoxynojirimycin (*N*B-DNJ).

### Neutralization assays

Neutralization activity of antibodies against pseudovirus in TZM-bl cells was determined as described previously[39]. Fold change in neutralization for PGT 135 mutants is summarized in Supplementary Table 10

### Antibody and envelope mutations

Mutations in the PGT heavy chain, the HIV-1envelope glycoprotein and the JRFLmV3 construct were introduced using QuikChange site-directed mutagenesis (Stratagene, La Jolla, CA). Mutations were verified by DNA sequencing (Eton Biosciences, La Jolla, CA).

### JR-FLmV3 glycan mutant binding ELISAs

JR-FLmV3 glycan mutants were expressed in 293S cells. Glycoproteins from the crude supernatant were captured onto ELISA plates using mAb 17b. Serial dilutions of biotinylated PGT 135 were added and antibody binding was probed with alkaline phosphatase conjugated streptavidin (Jackson, diluted to 1:1000) and visualized with *p*-nitrophenol phosphate substrate (Sigma) at 405 nm.

### High density high-mannose array printing

$Man_7GlcNAc_2$-Gly, $Man_8GlcNAc_2$-Gly, and $Man_9GlcNAc_2$Gly were printed in replicates of six onto NHS-activated glass slides (from ADA Technologies, Inc) at a concentration of 100 μM as previously described in ref. 13 using a MicroGridII contact microarray printing robot. Printing efficiency was determined by measuring ConA binding.

### Binding of antibodies to high-density high-mannose array

Binding of PGT 135, PGT128 and 2G12 antibodies was measured at 30 μg/mL and detected using goat-anti-human-Fcγ-R-PE (15 μg/mL, Jackson). Arrays were scanned for R-PE fluorescence on a ProScanArray HT (PerkinElmer) confocal slide scanner at 70PMT90LP. Signal intensities were collected using Imagene (BioDiscovery) image analysis software and calculated using the mean intensity of 4 replicate spotted samples.

### Comparison of PGT 135 binding to low density (Schott slides) and high-density (ADA slides) glycan microarrays

Glycan microarray analysis was initially carried out on high-mannose glycans printed on NHS-activated slides obtained from Schott as in ref. 13, but binding of PGT 135 could not be detected (Supplementary Fig. 5a). However, PGT 135 glycan binding could be detected (Supplementary Fig. 5a) using the glycan array imprinted on higher density NHS-activated slides from ADA Technologies, Inc. As a comparison, we show that binding of PGT128 was greatly enhanced using the high-density slides (Supplementary Fig. 5b) and strong binding on the array could still be detected at 1μg/mL.

### Neoglycolipid (NGL) microarray analyses

Analysis with neoglycolipid arrays was carried out as described previously in ref. 13. PGT 135 was pre-complexed with biotinylated anti-human-IgG (Vector) at a 1:3 ratio, w/w, before applying onto the slides at a final concentration of 10 μg/ml. Binding was detected with Alexa-Fluor 647 labeled streptavidin (Molecular Probes) at 1 μg/ml. Included for comparison are the results with human 2G12 (Polymun Scientific) taken from an earlier experiment performed using a different version of microarrays[40], PGT128 and plant lectin ConA in ref. 13 (Supplementary Table 8; Supplementary Fig. 5c)

### Electron microscopy and image processing

PGT 135 Fab in complex with the BG505 SOSIP.664 trimer used for electron microscopy studies were prepared as previously described in ref. 13. Particles were picked automatically using DoG Picker and put into a particle stack using the Appion software package[41,42]. Initial reference-free 2D class averages were calculated using particles binned by 4 via the Xmipp Clustering 2D Alignment[43], and IMAGIC software programs[44]. Particles were further classified into reference-free 2D class averages and refined using Refine2d in the EMAN package[45] (Supplementary Fig. 6a). An *ab initio* 3D model was generated by refining the EM map of an unliganded BG505 SOSIP.664 trimer for 29 iterations, against the 2D class averages from the last Refine2d iterations. This initial model was used for the final 75-iteration 3D refinement against 8,831 raw particles binned by 2 using EMAN[45]. C3 symmetry was imposed throughout the reconstruction process. The final 3D reconstruction has a resolution of 20 Å by an FSC cut-off at 0.5 (Supplementary Fig. 6b).

### Fitting of gp120/PGT 135 crystal structure into the EM density

Due to the high B-values in the constant region of the PGT 135 Fab, initial rigid body fitting of the crystal structure was done with only the gp120 and the variable region of the PGT 135 Fab (Supplementary Fig. 6c). This structure was manually fit into the EM density and refined using the UCSF Chimera ‘Fit in Map’ function. The crystal structure with the full Fab was then aligned to the fitted structure using the ‘Match’ command. The fitting of trimeric gp120-PGT 135 crystal structure was further refined using the ‘Fit in Map’ function resulting in a final correlation value of 0.91.

### Analysis of Fab binding degeneracy

Candidate top views of PGT 135-trimer and PGT128-trimer particles were subjected to two rounds of reference-free 2D class averaging using Xmipp Clustering 2D Alignment[43]. 2D class averages with the clearest top views of gp120 were selected from the PGT 135 and PGT128 alignments to be used as a template for the respective datasets. A circular mask was applied to conceal the Fabs, and the remaining particles from the second round of reference free 2D alignments were re-classified via IMAGIC Multi Reference Alignment, and IMAGIC Multivariate Statistical Analysis programs[44]. The 164 and 160 aligned particles for PGT 135 and PGT128 respectively, from best the 2D class average for each were selected for 2D principal component analysis (PCA). The PCA analysis was carried out through the Sparx package[46] using the first 5 eigenvectors. UCSF Chimera was used to create morph movies (Supplementary movies 1-2) between the average image and each of the eigenvectors to visualize the flexibility.

## Supplementary Material

Refer to Web version on PubMed Central for supplementary material.

## Acknowledgments

We thank X. Dai for help with data processing; J. Chittuluru for assistance with the 2D principal component analysis; D. Ekiert for initial cloning of PGT 135; R. Pejchal for initial cloning of soluble CD4 and the gp120 JRFL core construct; C. Poulsen and R. Wyatt from the Scripps Research Institute, La Jolla, California, USA for donation of 17b IgG; C. Arnold from the UK National Institute for Biological Standards and Control, Health Protection Agency for donation of ARP3119 monoclonal antibody CA13; M. Elsliger for computer support; C. Corbaci for help with preparing figures and movies; A. Irimia, C. Blattner, and M. Hong for discussions; and J. P. Verenini for help in manuscript formatting, and W. Koff for discussions and support. We also thank S.C. Arzberger, J. Zhang and ADA Technologies, Inc for supplying the high-density NHS-activated slides used for glycan microarray analysis; members of The Glycosciences Laboratory for their collaboration in the establishment of the neoglycolipid based microarray system, and Terry Butters and colleagues from the University of Oxford, UK for the glucosylated *N*-glycans. Work using the neoglycolipid system is supported by The Wellcome Trust (WT093378MA and WT099197MA) (T.F.), The UK Research Councils' Basic Technology Initiative ‘Glycoarrays’ (GRS/79268) (T.F.), EPSRC Translational Grant (EP/G037604/1) and NCI Alliance of Glycobiologists for Detection of Cancer and Cancer Risk (U01 CA128416) (T.F.). The electron microscopy data were collected at the National Resource for Automated Molecular Microscopy, which is supported by US National Institutes of Health (NIH) through the National Center for Research Resources' P41 program (RR017573) (A.B.W.) at the National Center for Research Resources. X-ray data sets were collected at the Advanced Light Source beamline 5.0.2 at the Berkeley Center for Structural Biology (BCSB) and the Advanced Photon Source beamline 23ID-B. The BCSB is supported in part by the NIH, the US NIH National Institute of General Medical Sciences (NIGMS), and the Howard Hughes Medical Institute. The Advanced Light Source is supported by the Director, Office of Science, Office of Basic Energy Sciences, of the U.S. Department of Energy under Contract No. DE-AC02-05CH11231. Use of the APS was supported by the US Department of Energy, Basic Energy Sciences, Office of Science, under contract no. DE-AC02-06CH11357. The GM/CA-CAT 23-ID-B beamline has been funded in whole or in part with federal funds from the US National Cancer Institute (NCI) (Y1-CO-1020) and NIGMS (Y1-GM-1104). This work was supported by the International AIDS Vaccine Initiative Neutralizing Antibody Center; by the Center for HIV/AIDS Vaccine Immunology (CHAVI-ID UM1 AI00663) (A.B.W., D.R.B., I.A.W.); by the HIV Vaccine Research and Design (HIVRAD) program (P01 AI832362 and R37 AI36082) (J.P.M., A.B.W., I.A.W.); by the University of California, San Diego, Center for AIDS Research (CFAR) (A.B.W.), an NIH-funded program (P30 AI036214), which is supported by the following NIH Institutes and Centers: US National Institute of Allergy and Infectious Disease, NCI, US National Institute of Mental Health, US National Institute on Drug Abuse, US National Institute of Child Health & Human Development, US National Institute of Heart, Lung and Blood, US National Institute of Aging; by NIH RO1 grant GM046192-18 (I.A.W.), and the Joint Center of Structural Genomics by the NIH, NIGMS, Protein Structure Initiative [U54 GM094586] (I.A.W.). A portion of the work is supported by an American Foundation for AIDS Research Mathilde Krim Fellowship in Basic Biomedical Research (L.K.). The content is the responsibility of the authors and does not necessarily reflect the official views of NIGMS, NCI or the NIH. This is manuscript #21722 from The Scripps Research Institute.

## References


1. Weiss RA, et al. Neutralization of human T-lymphotropic virus type III by sera of AIDS and AIDS-risk patients. Nature. 1985; 316:69–72. [PubMed: 2989706]
2. Wei X, et al. Antibody neutralization and escape by HIV-1. Nature. 2003; 422:307–312. [PubMed: 12646921]
3. Zhang M, et al. Tracking global patterns of N-linked glycosylation site variation in highly variable viral glycoproteins: HIV, SIV, and HCV envelopes and influenza hemagglutinin. Glycobiology. 2004; 14:1229–1246. [PubMed: 15175256]
4. Richman DD, Wrin T, Little SJ, Petropoulos CJ. Rapid evolution of the neutralizing antibody response to HIV type 1 infection. Proc Natl Acad Sci U S A. 2003; 100:4144–4149. [PubMed: 12644702]
5. Scheid JF, et al. Sequence and structural convergence of broad and potent HIV antibodies that mimic CD4 binding. Science. 2011; 333:1633–1637. [PubMed: 21764753]
6. Stamatatos L, Morris L, Burton DR, Mascola JR. Neutralizing antibodies generated during natural HIV-1 infection: good news for an HIV-1 vaccine? Nat Med. 2009; 15:866–870. [PubMed: 19525964]
7. Walker LM, et al. Rapid development of glycan-specific, broad, and potent anti-HIV-1 gp120 neutralizing antibodies in an R5 SIV/HIV chimeric virus infected macaque. Proc Natl Acad Sci U S A. 2011; 108:20125–20129. [PubMed: 22123961]
8. Gray ES, et al. The neutralization breadth of HIV-1 develops incrementally over four years and is associated with CD4+ T cell decline and high viral load during acute infection. J Virol. 2011; 85:4828–4840. [PubMed: 21389135]
9. Moore PL, et al. Evolution of an HIV glycan-dependent broadly neutralizing antibody epitope through immune escape. Nat Med. 2012; 18:1688–1692. [PubMed: 23086475]
10. Burton DR, et al. A Blueprint for HIV Vaccine Discovery. Cell Host Microbe. 2012; 12:396–407. [PubMed: 23084910]
11. Mouquet H, et al. Complex-type N-glycan recognition by potent broadly neutralizing HIV antibodies. Proc Natl Acad Sci U S A. 2012; 109:E3268–3277. [PubMed: 23115339]
12. Calarese DA, et al. Antibody domain exchange is an immunological solution to carbohydrate cluster recognition. Science. 2003; 300:2065–2071. [PubMed: 12829775]
13. Pejchal R, et al. A potent and broad neutralizing antibody recognizes and penetrates the HIV glycan shield. Science. 2011; 334:1097–1103. [PubMed: 21998254]
14. McLellan JS, et al. Structure of HIV-1 gp120 V1/V2 domain with broadly neutralizing antibody PG9. Nature. 2011; 480:336–343. [PubMed: 22113616]
15. Walker LM, et al. Broad and potent neutralizing antibodies from an African donor reveal a new HIV-1 vaccine target. Science. 2009; 326:285–289. [PubMed: 19729618]
16. Walker LM, et al. Broad neutralization coverage of HIV by multiple highly potent antibodies. Nature. 2011; 477:466–470. [PubMed: 21849977]
17. Zhu J, et al. Somatic populations of PGT135-137 HIV-1-neutralizing antibodies identified by 454 pyrosequencing and bioinformatics. Front Microbiol. 2012; 3:315. [PubMed: 23024643]
18. Kwong PD, et al. Probability analysis of variational crystallization and its application to gp120, the exterior envelope glycoprotein of type 1 human immunodeficiency virus (HIV-1). J Biol Chem. 1999; 274:4115–4123. [PubMed: 9933605]
19. Tong T, Crooks ET, Osawa K, Binley JM. HIV-1 virus-like particles bearing pure env trimers expose neutralizing epitopes but occlude nonneutralizing epitopes. J Virol. 2012; 86:3574–3587. [PubMed: 22301141]
20. Zhou T, et al. Structural definition of a conserved neutralization epitope on HIV-1 gp120. Nature. 2007; 445:732–737. [PubMed: 17301785]
21. Yang X, Lipchina I, Cocklin S, Chaiken I, Sodroski J. Antibody binding is a dominant determinant of the efficiency of human immunodeficiency virus type 1 neutralization. J Virol. 2006; 80:11404–11408. [PubMed: 16956933]

22. Burton DR, Saphire EO, Parren PW. A model for neutralization of viruses based on antibody coating of the virion surface. Curr Top Microbiol Immunol. 2001; 260:109–143. [PubMed: 11443871]

23. Zemlin M, et al. Expressed murine and human CDR-H3 intervals of equal length exhibit distinct repertoires that differ in their amino acid composition and predicted range of structures. J Mol Biol. 2003; 334:733–749. [PubMed: 14636599]

24. Kasturi L, Chen H, Shakin-Eshleman SH. Regulation of N-linked core glycosylation: use of a site-directed mutagenesis approach to identify Asn-Xaa-Ser/Thr sequons that are poor oligosaccharide acceptors. Biochem J. 1997; 323:415–419. [PubMed: 9163332]

25. Rudd PM, Dwek RA. Glycosylation: heterogeneity and the 3D structure of proteins. Crit Rev Biochem Mol Biol. 1997; 32:1–100. [PubMed: 9063619]

26. Binley JM, et al. Role of complex carbohydrates in human immunodeficiency virus type 1 infection and resistance to antibody neutralization. J Virol. 2010; 84:5637–5655. [PubMed: 20335257]

27. Sanders RW, et al. The mannose-dependent epitope for neutralizing antibody 2G12 on human immunodeficiency virus type 1 glycoprotein gp120. J Virol. 2002; 76:7293–7305. [PubMed: 12072528]

28. Fischer PB, et al. The α-glucosidase inhibitor N-butyldeoxynojirimycin inhibits human immunodeficiency virus entry at the level of post-CD4 binding. J Virol. 1995; 69:5791–5797. [PubMed: 7543588]

29. Julien JP, et al. Asymmetric recognition of the HIV-1 trimer by broadly neutralizing antibody PG9. Proc Natl Acad Sci U S A. 2013; 110:4351–4356. [PubMed: 23426631]

30. Liu J, Bartesaghi A, Borgnia MJ, Sapiro G, Subramaniam S. Molecular architecture of native HIV-1 gp120 trimers. Nature. 2008; 455:109–113. [PubMed: 18668044]

31. Chen L, et al. Structural basis of immune evasion at the site of CD4 attachment on HIV-1 gp120. Science. 2009; 326:1123–1127. [PubMed: 19965434]

32. Weis WI, Drickamer K. Structural basis of lectin-carbohydrate recognition. Annu Rev Biochem. 1996; 65:441–473. [PubMed: 8811186]

33. Azoitei ML, et al. Computation-guided backbone grafting of a discontinuous motif onto a protein scaffold. Science. 2011; 334:373–376. [PubMed: 22021856]

34. Guenaga J, et al. Heterologous epitope-scaffold prime:boosting immuno-focuses B cell responses to the HIV-1 gp41 2F5 neutralization determinant. PLoS ONE. 2011; 6:e16074. [PubMed: 21297864]

13. Pejchal R, et al. A potent and broad neutralizing antibody recognizes and penetrates the HIV glycan shield. Science. 2011; 334:1097–1103. [PubMed: 21998254]

35. Sanders RW, et al. Stabilization of the soluble, cleaved, trimeric form of the envelope glycoprotein complex of human immunodeficiency virus type 1. J Virol. 2002; 76:8875–8889. [PubMed: 12163607]

36. Hoffenberg S, et al. Identification of an HIV-1 Clade A Envelope from Protocol G virus sequence data that exhibits broad antigenicity and neutralization sensitvity and elicts antibodies targeting 3 distinct epitopes. J Virol. 201310.1128/JVI.02827-02812

37. Otwinowski Z, Minor W. Processing of X-ray diffraction data collected in oscillation mode. Methods Enzymol. 1997; 276:307–326.

38. Adams PD, et al. PHENIX: a comprehensive Python-based system for macromolecular structure solution. Acta Crystallogr Sect D Biol Crystallogr. 2010; 66:213–221. [PubMed: 20124702]

39. Li M, et al. Human immunodeficiency virus type 1 env clones from acute and early subtype B infections for standardized assessments of vaccine-elicited neutralizing antibodies. J Virol. 2005; 79:10108–10125. [PubMed: 16051804]

40. Dunlop DC, et al. Polysaccharide mimicry of the epitope of the broadly neutralizing anti-HIV antibody, 2G12, induces enhanced antibody responses to self oligomannose glycans. Glycobiology. 2010; 20:812–823. [PubMed: 20181792]

41. Lander GC, et al. Appion: an integrated, database-driven pipeline to facilitate EM image processing. J Struct Biol. 2009; 166:95–102. [PubMed: 19263523]

42. Voss NR, Yoshioka CK, Radermacher M, Potter CS, Carragher B. DoG Picker and TiltPicker: software tools to facilitate particle selection in single particle electron microscopy. J Struct Biol. 2009; 166:205–213. [PubMed: 19374019]

43. Sorzano CO, et al. A clustering approach to multireference alignment of single-particle projections in electron microscopy. J Struct Biol. 2010; 171:197–206. [PubMed: 20362059]

44. van Heel M, Harauz G, Orlova EV, Schmidt R, Schatz M. A new generation of the IMAGIC image processing system. J Struct Biol. 1996; 116:17–24. [PubMed: 8742718]

45. Ludtke SJ, Baldwin PR, Chiu W. EMAN: semiautomated software for high-resolution single-particle reconstructions. J Struct Biol. 1999; 128:82–97. [PubMed: 10600563]

46. Hohn M, et al. SPARX, a new environment for Cryo-EM image processing. J Struct Biol. 2007; 157:47–55. [PubMed: 16931051]

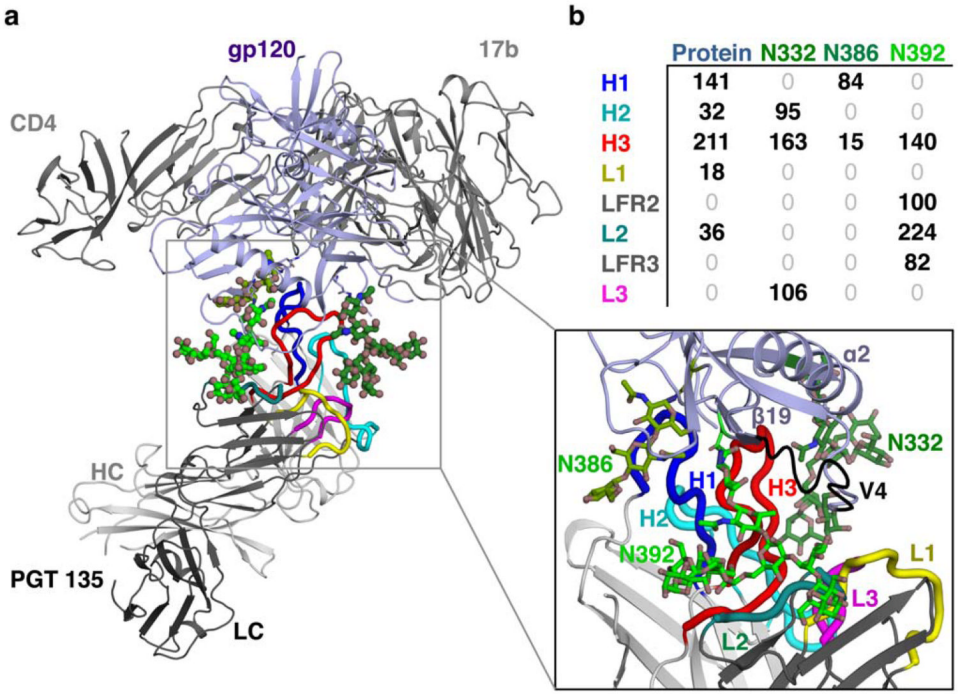


b

| | Protein | N332 | N386 | N392 |
|---|---|---|---|---|
| H1 | 141 | 0 | 84 | 0 |
| H2 | 32 | 95 | 0 | 0 |
| H3 | 211 | 163 | 15 | 140 |
| L1 | 18 | 0 | 0 | 0 |
| LFR2 | 0 | 0 | 0 | 100 |
| L2 | 36 | 0 | 0 | 224 |
| LFR3 | 0 | 0 | 0 | 82 |
| L3 | 0 | 106 | 0 | 0 |

**Figure 1. Crystal structure of PGT 135 in complex with HIV-1 gp120**

**(a)** The glycan-dependent interaction between PGT 135 and gp120 is presented in ribbon representation in the context of the gp120 ternary complex that contains a 2-domain CD4 and the Fab of CD4-induced antibody 17b. An enlarged display of the PGT 135-gp120 interaction is shown to the lower right. The CDR H1 and H3 loops (blue and red respectively) penetrate deeply through the glycan canopy to contact protein surface below while the light chain contacts the glycans using CDR loops and framework regions. **(b)** Buried surface on gp120 protein surface and attached glycans N332, N386 and N392 by CDR loops and framework regions of PGT 135. The values are in $Å^{2}$.

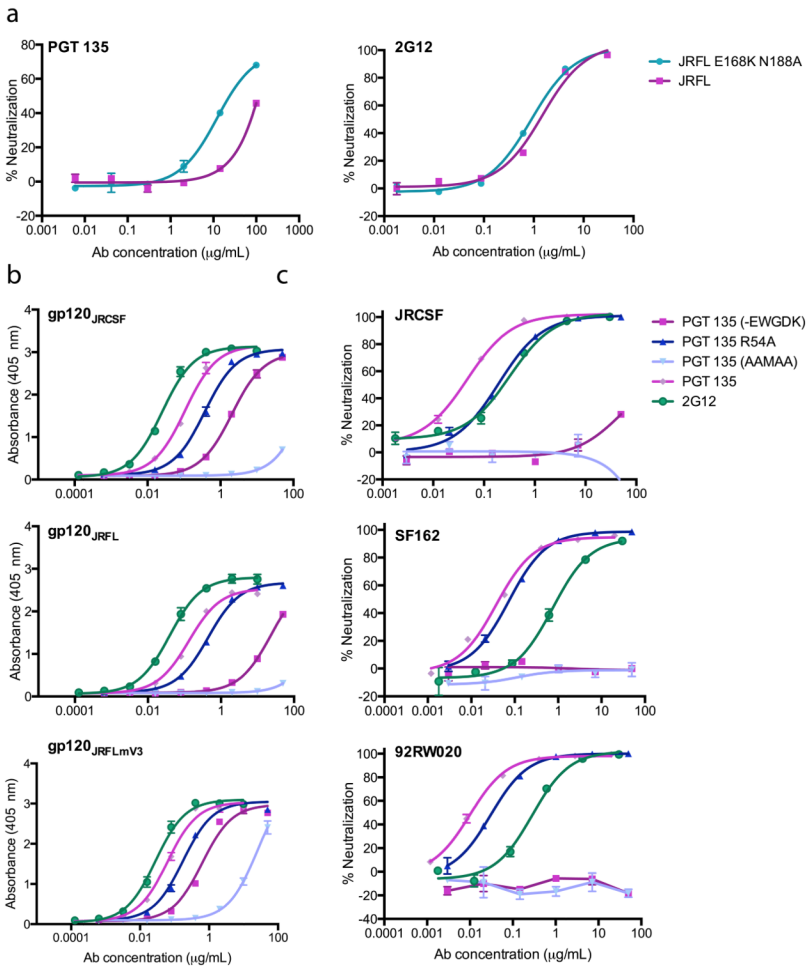


**Figure 2. PGT 135 neutralization and binding**

**(a)** Neutralization activity of PGT 135 and 2G12 were assayed against JR-FL pseudovirus in TZM-bl cells. Neutralization of WT JR-FL and of JR-FL containing V1-V2 loop mutations E168K and N188A are shown. **(b)** Binding of PGT 135 IgG mutants to gp120 from various strains (JRCSF, JRFL) as well as JRFLmV3 were measured by ELISA. Mutations include deletion of the CDR H1 insert "EWGDK", alanine substitution of the CDR H2 arginine that supports the CDR H1 insert with a salt bridge, and mutation of VFMLV to AAMAA in CDR H3. Wild-type PGT 135 and 2G12 IgGs are included as controls. **(c)** Neutralization potency of PGT 135 mutant IgGs against JRCSF, SF162 and 92RW020. Error bars represent the standard deviation. Experiments were performed in duplicate and repeated three times.

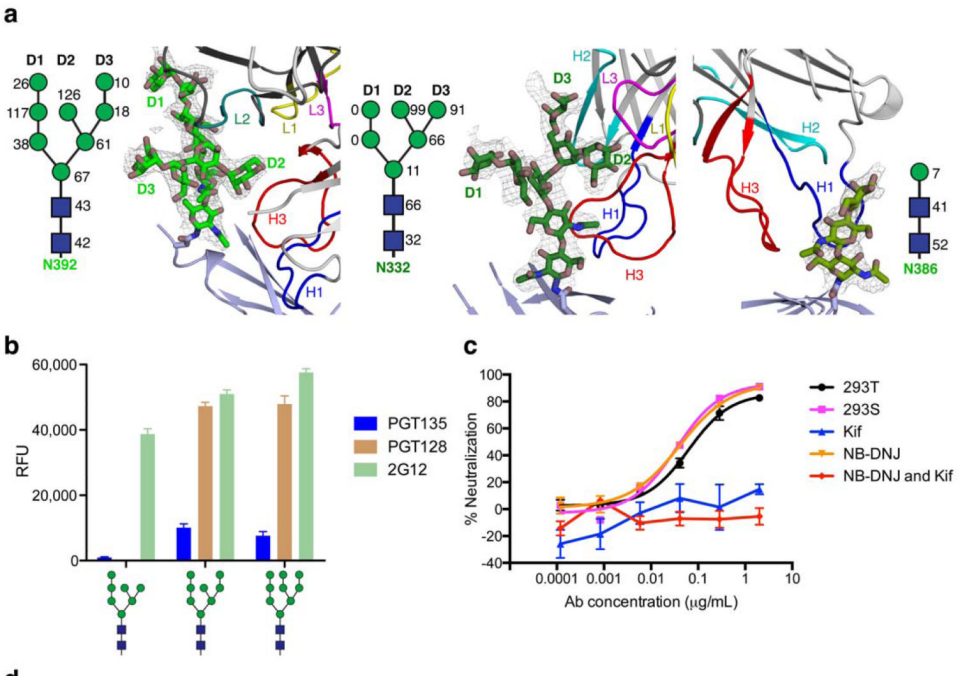


d

| Virus strain | N295A | N301A | H330A | N332A | N339A | N386A | N392A |
|---|---|---|---|---|---|---|---|
| JRCSF | 26 | 0.4 | >950 | >950 | 0.8 | 4.1 | >950 |
| 92RW020 | >2,000 | n.d. | 89.3 | >2,000 | 4.0 | >2,400 | >2,400 |
| SF162 | 0.9 | n.d. | 7.3 | >700 | 0.3 | >1,200 | >1,200 |
| JRFLmV3[a] | 0.7 | 0.7 | 10.1 | >600 | 0.8 | 1.1 | 49 |
| Bal | n.d. | n.d. | n.d. | >600 | n.d. | n.d. | n.d. |

**Figure 3. Glycan dependency of PGT 135 binding to gp120**

**(a)** PGT 135 interactions with gp120 glycans. The 2Fo-Fc electron density (contoured at 1σ) of N392, N332 and N386 glycans are shown along with contacting residues on PGT 135. A schematic of each glycan is shown beside the structures for the sugars that are visible in the electron density with GlcNAc as dark blue squares and mannose residues as green circles. The surface area (Å$^2$) on each glycan moiety buried by PGT 135 is shown. **(b)** Interactions of PGT 135, PGT 128 and 2G12 with oligomannose glycans on a high-density microarray. The error bars represent standard deviations where n=6. **(c)** Glycan dependency of PGT 135 neutralization using BaL pseudoviruses produced in different cell systems. Virus produced in 293T cells contains complex, hybrid and oligomannose type glycans, whereas in 293S cells only $Man_{5\text{-}9}GlcNAc_2$ glycans are present. Addition of kifunensine yields only $Man_9GlcNAc_2$ glycans. NB-DNJ blocks the glycan processing at neutral glucosylated glycans. Error bars represent the standard deviation. Each experiment was performed in duplicate and repeated at least three times. **(d)** The effect on PGT 135 neutralization from single mutations removing glycans and His330 for several HIV-1 strains. Values are presented as fold change in $IC_{50}$ of variant envelope compared to WT envelope (fold change = $IC_{50}$ variant/$IC_{50}$ WT). Boxes are color coded for fold change; red: >100, orange 10-100, yellow 4-9 and green <4. n.d.: not determined. [a] values were determined by ELISA instead of neutralization.

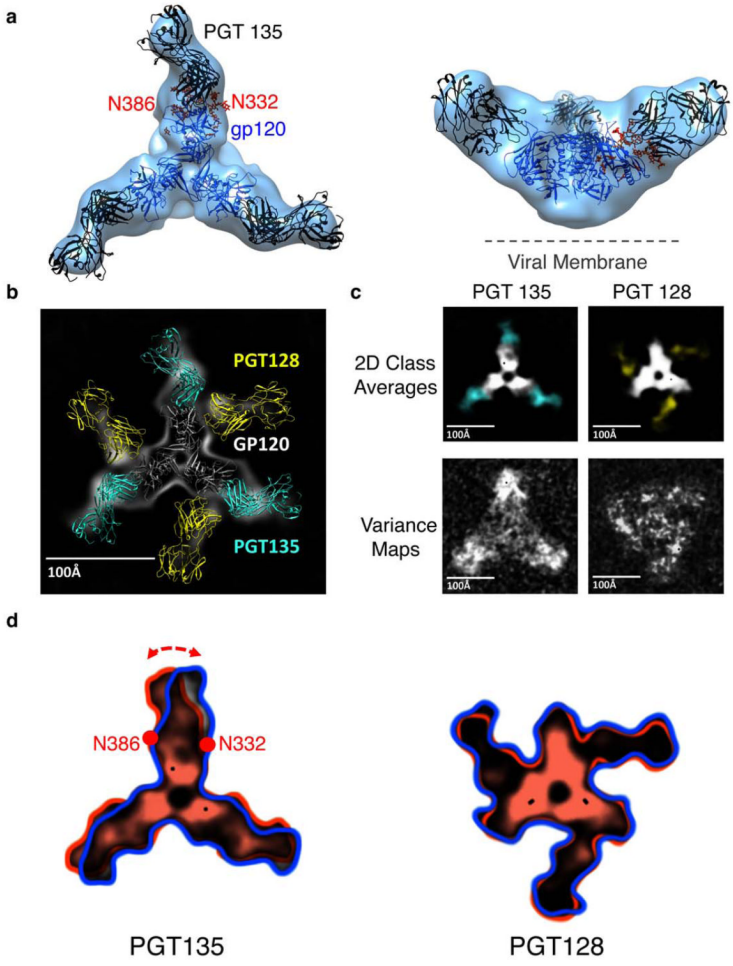


**Figure 4. A gp140 trimer binds Fab PGT 135 in slightly different orientations in contrast to PGT128, which is bound in a single orientation**

**(a)** The PGT 135-gp120 structure is shown fitted into the EM density map of PGT 135 in complex with the BG505 SOSIP.664 gp140 trimer in top and side views of the trimer. **(b)** 2D difference map of the two 2D class averages. The PGT128-SOSIP class average was subtracted from the PGT 135-SOSIP class average. The overlap is shown as the black gap in the trimer region. **(c)** Top view of the 2D class averages of the BG505 SOSIP.664 gp140 trimer in complex with PGT 135 (left) and PGT128 (right). The images contributing to the class averages were aligned using a top view back projection of an undecorated gp140 SOSIP.664 trimer. On the top, the Fabs are colored cyan and yellow for PGT 135 and PGT128, respectively. Below are variance maps of the trimer in complex with PGT 135 (left) and PGT128 (right) indicating the variability in the images that went into the 2D class averages. Brighter pixel values correspond to a greater degree of variability in that region. **(d)** An overlay of the 2D class average (blue outline) and the first eigenvector (orange) of the 2D PCA analysis for PGT 135 and PGT128.

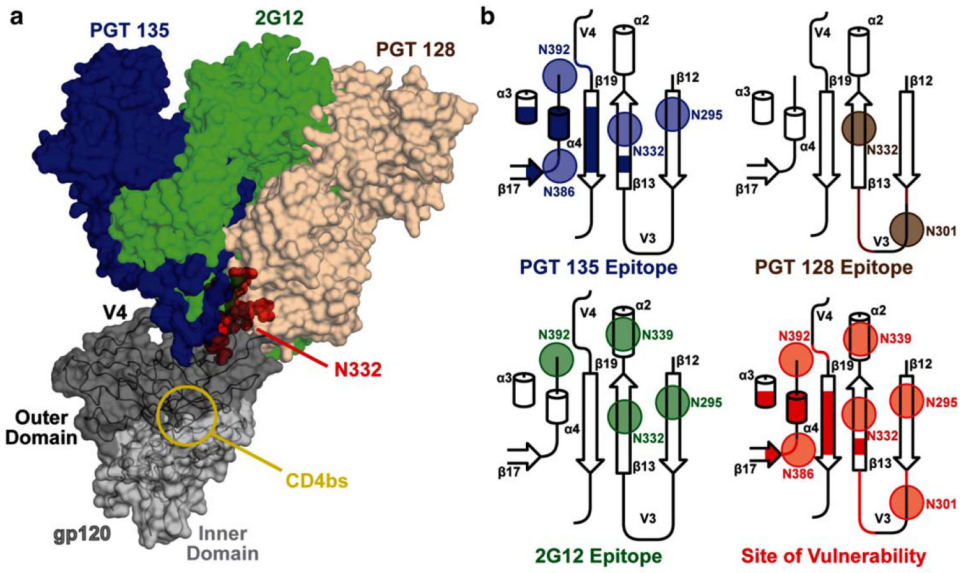


**Figure 5. Supersite of vulnerability centered on the N332 glycan**

**(a)** Binding to the N332 glycan on gp120 for PGT 135, 2G12 and PGT 128 is shown with their respective structures superimposed on glycan N332. **(b)** The epitopes of PGT 135, PGT 128 and 2G12 are shown in topology representations in which cylinders are α-helices, arrows are β-strands and lines are loops. *N*-linked glycan sites are circled. The structures of 2G12 (PDBID: 1OP5) and PGT 128 (PDBID: 3TYG) were obtained from the PDB.

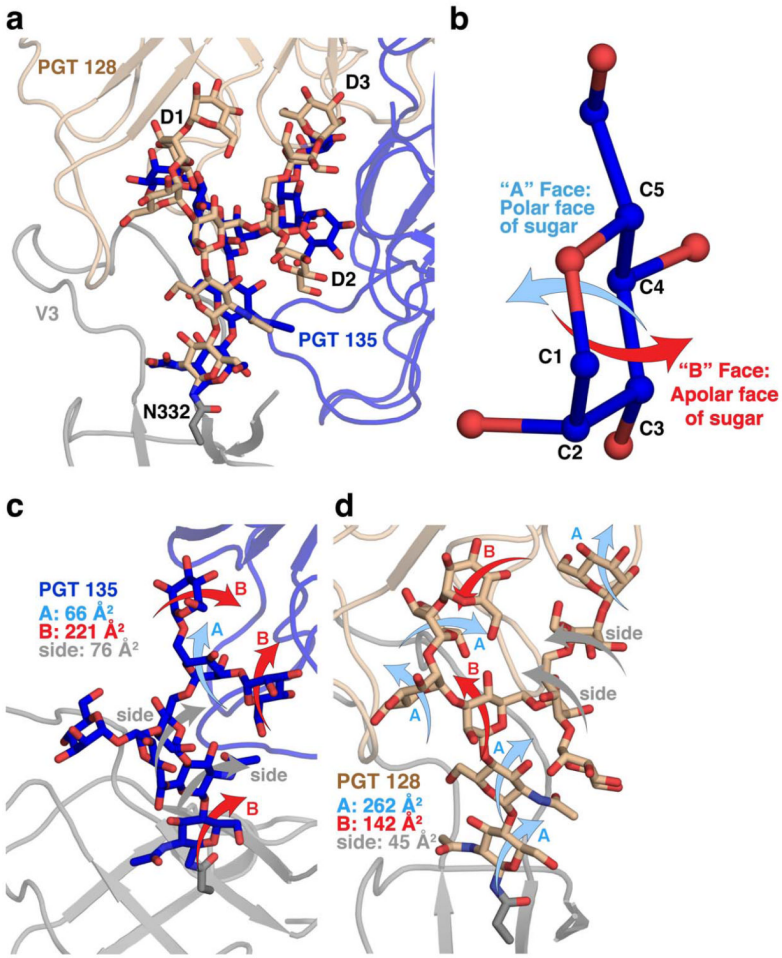


**Figure 6. Conserved conformation of N332 glycan**

**(a)** The *N*-linked glycan at N332 of gp120 has a conserved conformation in crystal structures with PGT 135 (blue) and PGT 128 (light brown). The structures are superposed on the gp120 protein. **(b)** Definition of A and B faces of a glycan residue. The B face (labeled in red), on which the carbons are arranged counter-clockwise around the ring, is generally more apolar than the A face (labeled in cyan), on which the carbons are arranged clockwise around the ring. **(c,d)** The side from which each glycan moiety interacts with PGT 135 **(c)** or PGT 128 **(d)** is defined by an arrow pointing towards the interaction (red arrow indicates B face, cyan arrow indicates A face and grey arrow indicates the side of a glycan). Each sugar primarily uses its A face, B face, or the side in the interaction with the different antibodies; their buried surface areas are estimated based on the burial on each glycan residue. The structure of PGT 128 (PDBID: 3TYG) is available from the PDB.

## Table 1
## Data collection and refinement statistics (molecular replacement)

| | PGT 135 | PGT 135-gp120-CD4-17b |
|---|---|---|
| **Data collection** | | |
| Space group | $P2_12_12$ | C2 |
| Cell dimensions | | |
| *a*, *b*, *c* (Å) | 85.89, 138.15, 42.34 | 218.41, 92.15, 88.19 |
| *α*, *β*, *γ* (°) | 90.00, 90.00, 90.00 | 90.00, 104.75, 90.00 |
| Resolution (Å) | 31.4-1.75 | 43.58-3.10 |
| | (1.78-1.75)[a,b] | (3.20-3.10)[a,b] |
| $R_{sym}$ | 0.06 (0.47) | 0.06 (0.60) |
| $I/\sigma I$ | 27.6 (1.9) | 16.9 (1.72) |
| Completeness (%) | 96.1 (73.8) | 99.7 (98.8) |
| Redundancy | 6.5 (4.0) | 3.7 (3.3) |
| **Refinement** | | |
| Resolution (Å) | 31.40-2.75 | 43.58-3.10 |
| No. reflections | 49,464 | 30,850 |
| $R_{work}/R_{free}$ | 20.7/24.5 | 24.6/36.7 |
| No. atoms | | |
| Protein | 3475 | 10,560 |
| Glycan/Ligand/ion | | 347 |
| Water | 273 | 1 |
| *B* factors | | |
| All proteins | 41 | 127 |
| gp120 | | 117 |
| 17b Fab | | 129 |
| CD4 D1D2 | | 149 |
| PGT135 con [c] | 43 | 151 |
| PGT135 var [c] | 39 | 99 |
| Glycans | | 112 |
| Ligands | | 109 |
| Water | 46 | 76 |
| r.m.s. deviations | | |
| Bond lengths (Å) | 0.006 | 0.012 |
| Bond angles (°) | 1.11 | 1.46 |

[a] One crystal for each structure was used for data collection and structure determination.

[b] Values in parentheses are for highest-resolution shell.

[c] For PGT 135 Fab, average B-values for the constant (con) and variable (var) domains were calculated.